Journal of Magnetic Resonance 212 (2011) 320–329

Contents lists available at SciVerse ScienceDirect

Journal of Magnetic Resonance

journal homepage: www.elsevier.com/locate/jmr

Broad-band homo-nuclear correlations assisted by ^{1}H irradiation for bio-molecules in very high magnetic field at fast and ultra-fast MAS frequencies

Bingwen Hu [a,*], Oliver Lafon [b], Julien Trébosc [b], Qun Chen [a], Jean-Paul Amoureux [b,*]

[a] Physics Department, Shanghai Key Laboratory of Magnetic Resonance, East China Normal University, Shanghai 200062, China
[b] UCCS, Lille North of France University, Villeneuve d'Ascq 59652, France

ARTICLE INFO

Article history:
Received 26 March 2011
Revised 11 July 2011
Available online 23 July 2011

Keywords:
Solid-state NMR
Indirect homo-nuclear correlation
Bio-molecules
Ultra-fast MAS
Very-high magnetic field

ABSTRACT

We propose a new broadband second-order proton-assisted ^{13}C–^{13}C correlation experiment, SHANGHAI. The ^{13}C–^{13}C magnetization transfer is promoted by ^{1}H irradiation with interspersed four phases supercycling. This through-space homo-nuclear sequence only irradiates on the proton channel during the mixing time. SHANGHAI benefits from a large number of modulation sidebands, hence leading to a large robustness with respect to chemical shift differences, which permits its use in a broad MAS frequency range. At ultra-fast MAS ($\nu_R \geqslant 60$ kHz), SHANGHAI is only efficient when the amplitude of ^{1}H recoupling rf-field is close to half the spinning speed ($\nu_1 \approx \nu_R/2$). However, at moderate to fast MAS ($\nu_R = 20$–35 kHz), SHANGHAI is efficient at any rf-power level larger than $\nu_1 \approx 10$ kHz, which simultaneously permits avoiding excessive heating of bio-molecules, and using large sample volumes. We show that SHANGHAI can be employed at the very high magnetic field of 23.5 T and then allows the observation of correlation between ^{13}C nuclei, even if their resonance frequencies differ by more than 38 kHz.

1. Introduction

Over the last approximately 10 years, Solid-State Nuclear Magnetic Resonance (SS-NMR) has become an important tool for structural investigations of proteins. Indeed, recent advances in SS-NMR techniques have made possible the complete structural determination of micro-crystalline proteins [1–4]. A key tool for the protein structural determination by SS-NMR is the observation of ^{13}C–^{13}C through-space proximities in fully ^{13}C-labeled proteins through the use of two-dimensional (2D) correlation experiments. The prominent role of ^{13}C 2D correlations is owed to (i) its ubiquity in the protein skeleton, (ii) its decent gyromagnetic ratio, (iii) its large chemical-shift range, and (iv) the high-resolution of ^{13}C spectra under magic-angle spinning (MAS). Nevertheless, for uniformly ^{13}C-labeled large bio-molecules, such as proteins, high magnetic fields ($B_0 > 14$ T) are usually required to obtain sufficient spectral resolution. Furthermore, at $B_0 \geqslant 18.8$ T, the spinning sidebands of aromatic ^{13}C sites displaying anisotropic chemical deshielding constant as large as 120 ppm can only be suppressed by the use of MAS frequencies, ν_R, larger than c.a. 24 kHz. Therefore, at $B_0 \geqslant 18.8$ T, rotor with a diameter smaller than 3.2 mm must be employed in order to suppress all chemical shift anisotropy (CSA) spinning sidebands. Furthermore, the difference in isotropic chemical shifts, $\Delta\delta_{iso}$, between carbonyl (C′) and aliphatic (C^{al}) sites can be as large as $\Delta\delta_{iso} \approx 170$ ppm. At $B_0 = 21.1$ T, this maximum value corresponds to a difference in resonance frequencies of $\Delta\nu_{iso}^{max} \approx 39$ kHz and the $\Delta\nu_{iso}$ values for all different cross-peaks span the whole interval [0, 39 kHz], as shown in Fig. 1. In an ideal ^{13}C–^{13}C through-space correlation 2D experiment, the intensity of cross-peaks should be independent of $\Delta\delta_{iso}$ values over the range [0, 170 ppm]. The development of such broadband methods is a current challenge of SS-NMR methodology.

The ^{13}C–^{13}C through-space correlation 2D experiments serve two purposes: the assignment of ^{13}C resonances and the determination of protein folding. The most efficient strategy for the assignment consists in the use of first-order dipolar recoupling schemes, such as SPC-5 [5,6], DREAM [6,7], CMpRR [8], fp-RFDR [6,9], and $BR2_2^1$ [10]. As these sequences are affected by dipolar truncation, the large dipolar couplings average the small ones [11,12]. Consequently, for short recoupling time, the first-order methods permit the selective observation of one-bond cross-peaks, which facilitates the assignment of ^{13}C resonance in the protein skeleton.

The three-dimensional structure determination of uniformly ^{13}C-labeled proteins requires the use of dipolar recoupling methods with attenuated or quenched dipolar truncation. Different strategies have been considered. One way is to use frequency-selective methods, such as Rotational Resonance (R^2) [13], COMICS [14], DQ-SEASHORE [15], and MIRROR [16]. A second way is to produce an Ising-type form for the dipolar Hamiltonian. These methods include the Truncated Dipolar Recoupling [17], the

* Corresponding authors. Fax: +33 3 20 43 68 14 (J.-P. Amoureux).
E-mail addresses: bwhu@phy.ecnu.edu.cn (B. Hu), jean-paul.amoureux@univ-lille1.fr (J.-P. Amoureux).

1090-7807/$ - see front matter © 2011 Elsevier Inc. All rights reserved.
doi:10.1016/j.jmr.2011.07.011

multiple-oscillating-field techniques [18], and the ZQ-SEASHORE [19]. A third way is to produce a stochastic Hamiltonian [20]. However, all these very recent broad-band methods [17–20] need to be brought to a better level of maturity. A fourth approach to attenuate the dipolar truncation relies on the use of second-order recoupling schemes. Most of these 2D methods are based on the same three-step scheme (Fig. 2a): (i) after evolution of the single-quantum (1Q) ^{13}C coherences during t_1, the carbon magnetization is stored along the B_0 axis, (ii) during the mixing period (τ_{mix}) diffusion process and/or proton-assisted homo-nuclear recoupling generate transfer of longitudinal magnetization between the different ^{13}C nuclei, and (iii) at the end of τ_{mix} a 90° pulse converts back the longitudinal ^{13}C magnetization into 1Q coherences which

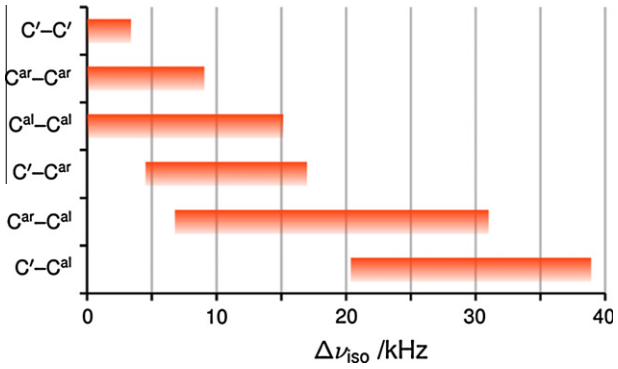

Fig. 1. Schematic distribution of $\Delta\nu_{iso}$ difference at 21.1 T for the ^{13}C–^{13}C cross-peaks between the different ^{13}C sites in peptides and proteins. The carbon nuclei are noted C′, C^{ar} and C^{al} for carbonyl, aromatic and aliphatic sites, respectively. For each type of cross-peak, the range of $\Delta\nu_{iso}$ is represented by a rectangle. The schematic distribution of $\Delta\nu_{iso}$ difference was calculated using the following isotropic chemical shift range: $170 \leqslant \delta_{iso}$ (C′) $\leqslant 185$ ppm, $110 \leqslant \delta_{iso}$ (C^{ar}) $\leqslant 150$ ppm, $13 \leqslant \delta_{iso}$ (C^{al}) $\leqslant 80$ ppm.

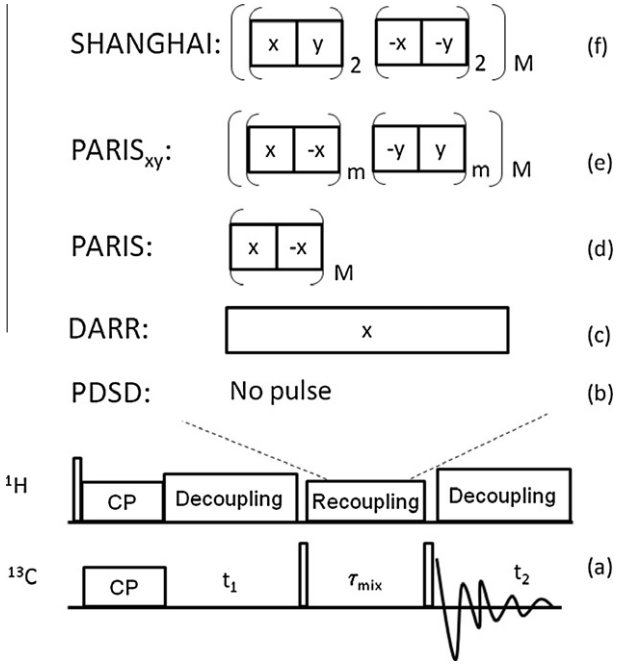

Fig. 2. (a) General scheme of the 2nd-order ^{13}C–^{13}C correlation experiments without ^{13}C irradiation during the mixing period. (b) PDSD, (c) DARR/RAD and MIRROR, (d) PARIS, (e) $PARIS_{xy}$ ($m = 1, 2$), (f) SHANGHAI. In (d–f) each pulse length is equal to $T_R/2$.

evolve during the acquisition period, t_2. Presently, such second-order recoupling sequences include the Proton Driven Spin Diffusion (PDSD) (Fig. 2b) [21–23], the Dipolar Assisted Rotational Resonance (DARR) [24] and its akin version Rf-Assisted Diffusion (RAD) [25] (Fig. 2c), and the Phase-Alternated Recoupling Irradiation Schemes: PARIS [26] (Fig. 2d) and $PARIS_{xy}$ (Fig. 2e) [27]. Strictly speaking, the DARR and RAD experiments employ radio-frequency (rf) nutation frequency, ν_1, equal to ν_R or $2\nu_R$. Nevertheless, continuous wave (CW) ^1H irradiation with other ν_1 values are able to promote efficient magnetization transfers owing to the resonance interference recoupling [24b], also called MIxed Rotational and ROtary Resonance (MIRROR) conditions [16]. For the sake of conciseness, in the following, the DARR experiment will refer to any ^{13}C–^{13}C dipolar recoupling assisted by CW ^1H irradiation. PARIS recoupling employing pulse lengths of half rotor period corresponds to the symmetry-based sequence $C1^0_1$ ($\theta_0\ \theta_{180}$), where θ_φ indicates a rectangular, resonant rf pulse with flip angle θ and phase φ with angles written in degrees. The m parameter of $PARIS_{xy}$ sequences is the number of alternations between opposite phases comprised between two $\pi/2$ phase shifts (see Fig. 2e). If the rf-field is equal to ν_R, the pulses are inversion elements and PARIS, $PARIS_{xy}$ ($m = 1$) and $PARIS_{xy}$ ($m = 2$) schemes correspond to the symmetries $[R2^1_1]_{270}$, $[R2^1_1]_{270}[R2^1_1]_{180}$ and $[R4^2_2]_{270}[R4^2_2]_{180}$.[28]. Here the subscripts after the brackets denotes overall phase shifts of the scheme inside the brackets.

In this article, we introduce a new recoupling sequence close to the $PARIS_{xy}$ ($m = 2$) scheme, the only difference being the succession order of the four phases, x, y, $-x$, and $-y$ (see Fig. 2f). We call this sequence: SHANGHAI, because the recoupling results from a Second-order Hamiltonian among Analogous Nuclei Generated by Hetero-nuclear Assistance Irradiation.

2. Simulations

The simulations were performed using SPINEVOLUTION software [29]. The powder averaging was accomplished using 1680 orientations (168 {α_{MR}, β_{MR}}-pairs × 10 γ_{MR}-angles). The 168 {α_{MR}, β_{MR}}-pairs, which relate the molecular and rotor frames, were selected according to the REPULSION algorithm [30]. Simulations presented in Figs. 3 and 4, and S1 were performed on a C1H–C2 spin-system, where the inter-nuclear distances are r(C1–C2) = 153.2 pm, r(C1–H) = 107.9 pm and r(C2–H) = 215.2 pm. For all the simulations presented in the article, the CSAs of ^{13}C and ^1H nuclei were zero, but we have observed (not shown) that the polarization transfer conditions in Figs. 3 and 4, and S1 are broadened by their introduction. To test the effect of ^1H–^1H dipolar interactions, similar simulations were performed for C1H–$C2H_2$–H_2 spin system (see Fig. 5 and Section 2.3). For this spin system, the inter-nuclear distances are those between the aliphatic sites in a crystal of L-glutamine with C1H = $C^\alpha H^\alpha$, $C2H_2 = C^\beta H^\beta_2$ and $H_2 = H^\gamma_2$. In the simulations, all protons have identical isotropic chemical shifts, and on-resonance irradiation was applied to the ^1H channel. The difference in resonance frequencies, $\Delta\nu_{iso}$, between the C1 and C2 nuclei was varied between 0 and values slightly larger than the MAS frequency, ν_R. Such an interval allows the observation of all the relevant magnetization transfer conditions. Simulations were performed at MAS frequencies of 32 and 64 kHz. The pulse length was equal to half rotor period for PARIS, $PARIS_{xy}$ and SHANGHAI methods and the mixing time was $\tau_{mix} = 250$ ms. The radio-frequency (rf) nutation frequency, ν_1, was varied between 0 and values slightly larger than ν_R. Figs. 3–5 plot the efficiency of the magnetization transfer from the C1 to the C2 site as function of $\Delta\nu_{iso}$, and ν_1 frequencies. This efficiency is defined as the amplitude of the cross-peak for $\tau_{mix} = 250$ ms divided by the amplitude of the diagonal peak for $\tau_{mix} = 0$.

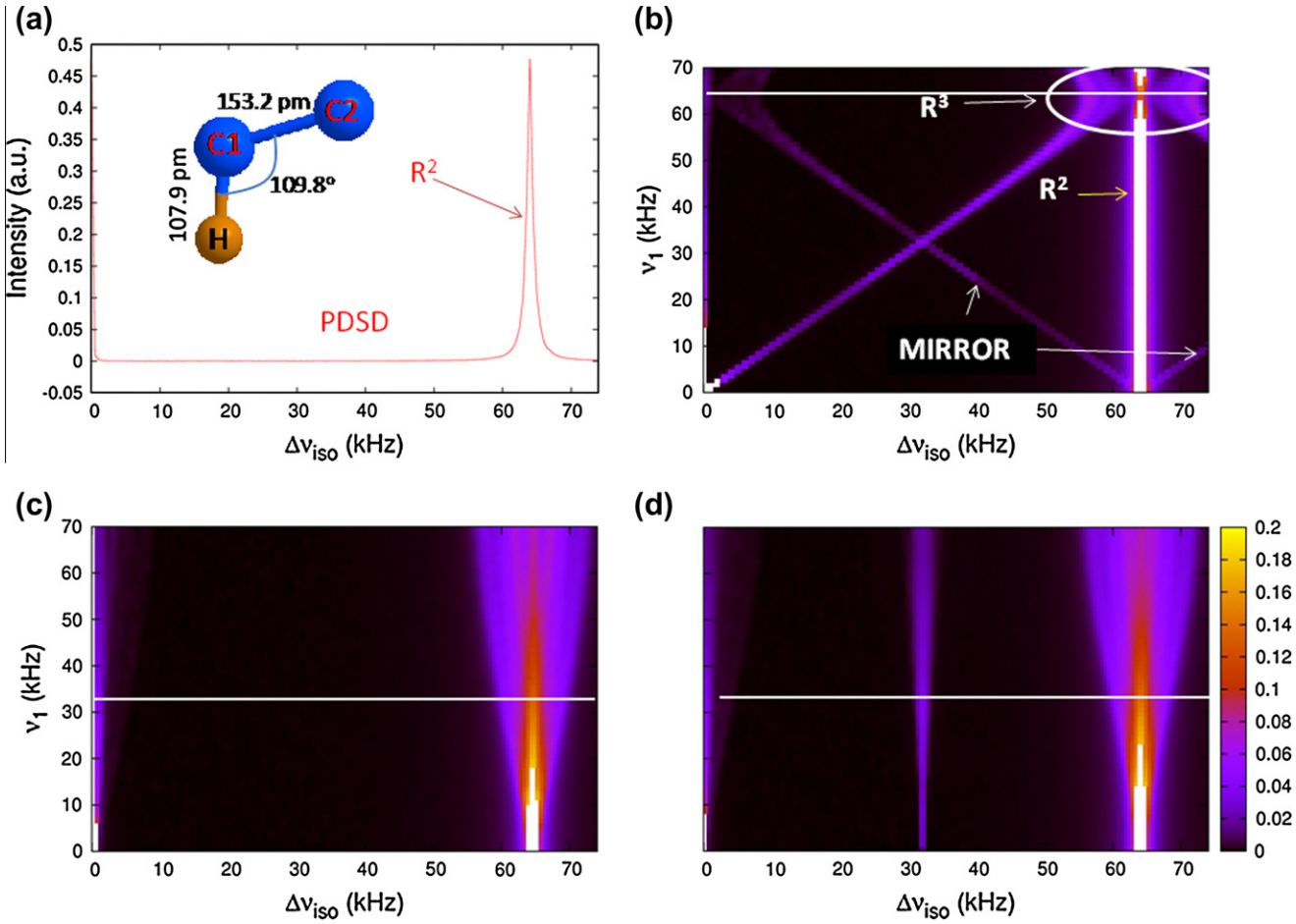

Fig. 3. Simulated recoupling efficiency of the ^{1}H assisted ^{13}C–^{13}C recoupling sequences versus the rf-field amplitude, ν_1, and the carbon frequency difference, $\Delta\nu_{iso}$. The following ^{13}C–^{13}C recoupling sequences were used: (a) PDSD, (b) DARR/RAD and MIRROR, (c) PARIS, (d) PARIS$_{xy}$ ($m = 1$). The spin-system is C1H–C2 and $\nu_R = 64$ kHz. We have limited the color representation to 0.2. When the efficiency is larger than 0.2, the zone is indicated in white. These high efficiencies are obtained around the R^{2}B and ZB conditions. The display limit of 0.2 allows emphasizing the foot of R^{2}B and ZB as well as the SBs. The maximum signal is always observed at $\Delta\nu_{iso} = \nu_R$ and it reaches 0.35 for (a) and 0.25 (b–d). In (b–d) a horizontal white line shows the position of the rows shown in Fig. S1.

2.1. C1H–C2 spin-system under ultra-fast MAS

MAS frequencies larger than 50 kHz and hence small rotor diameters offer several advantages for the study of proteins: (i) efficient low-power hetero-nuclear decoupling, which allows avoiding rf heating and is especially advisable in the case of aqueous, fragile biological systems with high salt concentration and high dielectric constant [31], (ii) enhanced sensitivity by the use of ^{1}H indirect detection under high-resolution [32], (iii) high sensitivity per spin, which is advantageous for volume-limited samples, such as isotopically labeled bio-molecules, and (iv) enhancement in sensitivity and resolution for paramagnetic proteins [33]. In Figs. 3, 4a, and b, the magnetization transfer efficiencies of the second-order recoupling sequences displayed in Fig. 2 were calculated for C1H–C2 spin-system at $\nu_R = 64$ kHz. They are plotted versus $\Delta\nu_{iso}$ frequency difference and rf-amplitude ν_1 for sequences other than PDSD. Indeed, in PDSD sequence, no pulse is sent during the mixing period (Fig. 2b) and the ^{13}C signal is transferred via the proton-assisted carbon–carbon flip-flop terms [22]. PDSD presents two cases of good efficiency which occur when the frequency difference is either small ($\Delta\nu_{iso} \approx 0$), or when it meets the very narrow R^2 condition, $\Delta\nu_{iso} = \nu_R$, [13] (Fig. 3a). It must be reminded that the R^2 recoupling leads to a broadening of the resonances and hence the exact matching condition, $\Delta\nu_{iso} = \nu_R$, should be avoided in case of proteins which always present crowded ^{13}C spectra. PDSD is mostly used under quasi-static conditions ($\nu_R < 7$ kHz) because its efficiency largely decreases when the MAS speed increases.

The DARR and RAD sequences (Fig. 2c) have been proposed to facilitate the ^{13}C–^{13}C recoupling by using a continuous-wave proton irradiation. Fig. 3b shows the recoupling efficiency of DARR versus the rf-field amplitude, ν_1, and the $\Delta\nu_{iso}$ frequency difference. In the following, we will call R^{2}B, ZB and SB the R^2-Band ($\Delta\nu_{iso} \approx \nu_R$), Zero-Band ($\Delta\nu_{iso} \approx 0$), and the other Side-Band recoupling conditions, respectively. Four bands are observable in Fig. 3b, three weak oblique SBs and the R^{2}B. Two oblique SBs correspond to the MIRROR conditions, $\nu_1 = \nu_R \pm \Delta\nu_{iso}$ [16], and the third MIRROR condition, $\nu_1 = \Delta\nu_{iso}$, corresponds to the overlap of the modulation sideband of one carbon site with the resonance of the other carbon. When ν_1 is smaller than ν_R, the R^{2}B condition is narrow and similar to that observed under exact R^2 condition. So, for $\nu_1 \leqslant \nu_R$, the only advantage of DARR sequence over PDSD is the presence of the three additional SBs. However, the DARR sequence also benefits from a broad recoupling zone, observed when $\nu_1 \approx \nu_R$ and circled in Fig. 3b, which corresponds to the rotary resonance recoupling (R^3) $n = 1$ condition [34], and is the really used DARR condition [24]. Under this condition, all the ^{1}H–^{13}C and ^{1}H–^{1}H dipolar interactions are reintroduced and efficient polarization transfer occurs if the spinning sideband of one carbon site overlaps the recoupled hetero-nuclear dipolar coupling pattern of the other carbon sites

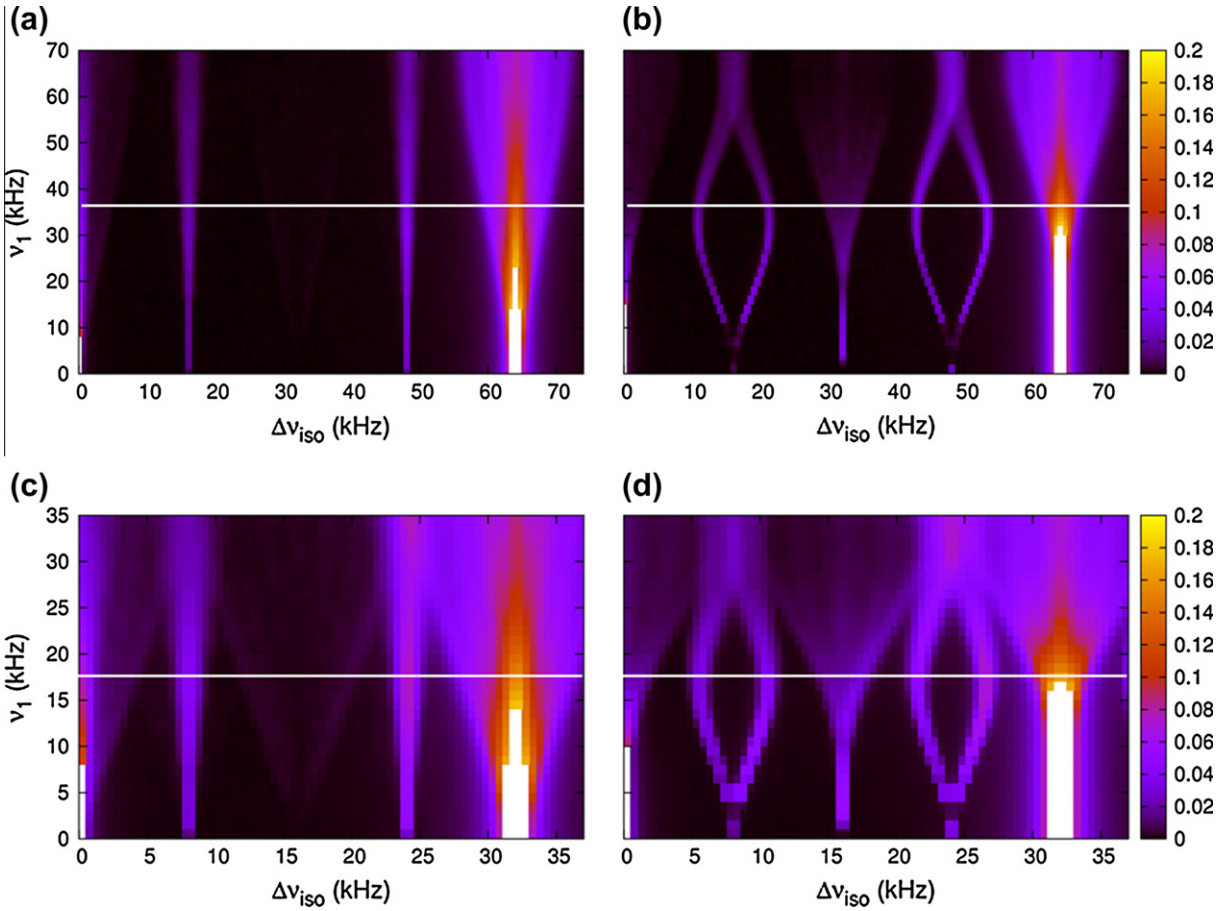

Fig. 4. Simulated recoupling efficiency of the sequences versus the rf-field amplitude, ν_1, and the carbon frequency difference, $\Delta\nu_{iso}$, at $\nu_R = 64$ (a and b) or 32 (c and d) kHz. The ^{13}C–^{13}C recoupling sequences are PARIS$_{xy}$ ($m = 2$) for (a and c) and SHANGHAI for (b and d). The spin-system is C1H–C2. The maximum signal is always observed at $\Delta\nu_{iso} = \nu_R$ and it reaches 0.3 for (a, b, and d), and 0.25 (c). In (b–d) a horizontal white line shows the position of the rows shown in Fig. S1.

[24]. The frequency width of the DARR condition is determined by the ^1H–^{13}C and ^1H–^1H dipolar couplings. However, Figs. 3b and S1a of Supplementary information show that even under the DARR condition, the efficiency exhibits a strong dependence on $\Delta\nu_{iso}$. Therefore, the DARR experiment is inefficient as soon as the ν_R frequency exceeds the maximal $\Delta\nu_{iso}$ values since there are no efficient recoupling condition for $0 < \Delta\nu_{iso} < \nu_R$ [28]. In addition, the sensitivity of R^3 to rf-inhomogeneity decreases in practice the efficiency of DARR experiments [26], as only a small part of the rotor fulfills the R^3 conditions and contributes to the cross-peak intensity. Another limitation of DARR experiment is that the condition $\nu_R \approx \Delta\nu_{iso} \approx \nu_1$ entails the use of high rf-power at high MAS frequency, which may denaturate the proteins.

The PARIS sequence, which has recently been proposed, employs phase-alternated $(x, -x)$ pulses with the length equal to half the rotor period (Fig. 2d) [26]. Fig. 3c shows that with respect to DARR, PARIS, which is an amplitude-modulated sequence, benefits from a lower dependence of ZB and R^2B transfer efficiency on the ν_1 rf-amplitude, which means also a lower dependence on the rf-inhomogeneity. The better robustness of R^2B condition results from the matching of the PARIS modulation frequency with the MAS frequency as the pulses last $T_R/2$ [26]. Furthermore, this lower dependence with the rf-amplitude ν_1 permits the use of weaker rf-power, which minimizes the risk of proteins denaturation (see Fig. S1a and b). In addition, the R^2B zone is much broader than the narrow exact R^2 condition, which allows efficient homo-nuclear magnetization transfer without deleterious line broadening. This wide R^2B zone, which is also observed for PARIS$_{xy}$ and SHANGHAI methods (vide infra), is partly responsible for the higher efficiency of these techniques with respect to DARR. It is interesting to note that with increasing rf-value, the effective R^2B region broadens around ν_R.

The PARIS$_{xy}$ sequences have been proposed very recently to further broaden the rf-matching profile of PARIS, while keeping the same robustness with respect to rf-inhomogeneity [27]. They also use half rotor-period phase-alternated ^1H pulses with x or y phases and an additional super-cycling that depends on the m value (see Fig. 2e). The efficiencies of magnetization transfer as function of ν_1 and $\Delta\nu_{iso}$ are displayed in Figs. 3d and 4a for PARIS$_{xy}$ sequences with $m = 1$ or 2, respectively. In addition to the ZB and R^2B already observed for the previously described methods, PARIS$_{xy}$ introduces one SB at $\Delta\nu_{iso}/\nu_R \approx 1/2$ when $m = 1$ and two SBs at $\Delta\nu_{iso}/\nu_R \approx 1/4$ and 3/4 when $m = 2$, see Fig. S1c and d, respectively. Furthermore, Figs. 3d and 4a show that as PARIS, PARIS$_{xy}$ displays a weak dependence on ν_1 frequency.

To further improve the robustness to isotropic chemical shift of ^{13}C–^{13}C dipolar recoupling assisted by ^1H irradiation, we introduce here the SHANGHAI sequence. Its super-cycling was derived using Floquet theory [35] in order to produce, for weak rf-field, many recoupling conditions in the useful region for ^{13}C–^{13}C correlations: $\Delta\nu_{iso} \leqslant \nu_R$. Actually, in addition to the ZB and R^2B, there exist mathematically eight SBs, which can be grouped in five SB zones, as shown in Fig. 4b. The HORROR condition, $\nu_1 = \nu_R/2$, which restores the ^1H–^1H dipolar interaction in the first-order average Hamiltonian, also results in the largest spread in $\Delta\nu_{iso}$ positions between the five SB zones. A comparison of the magnetization transfer

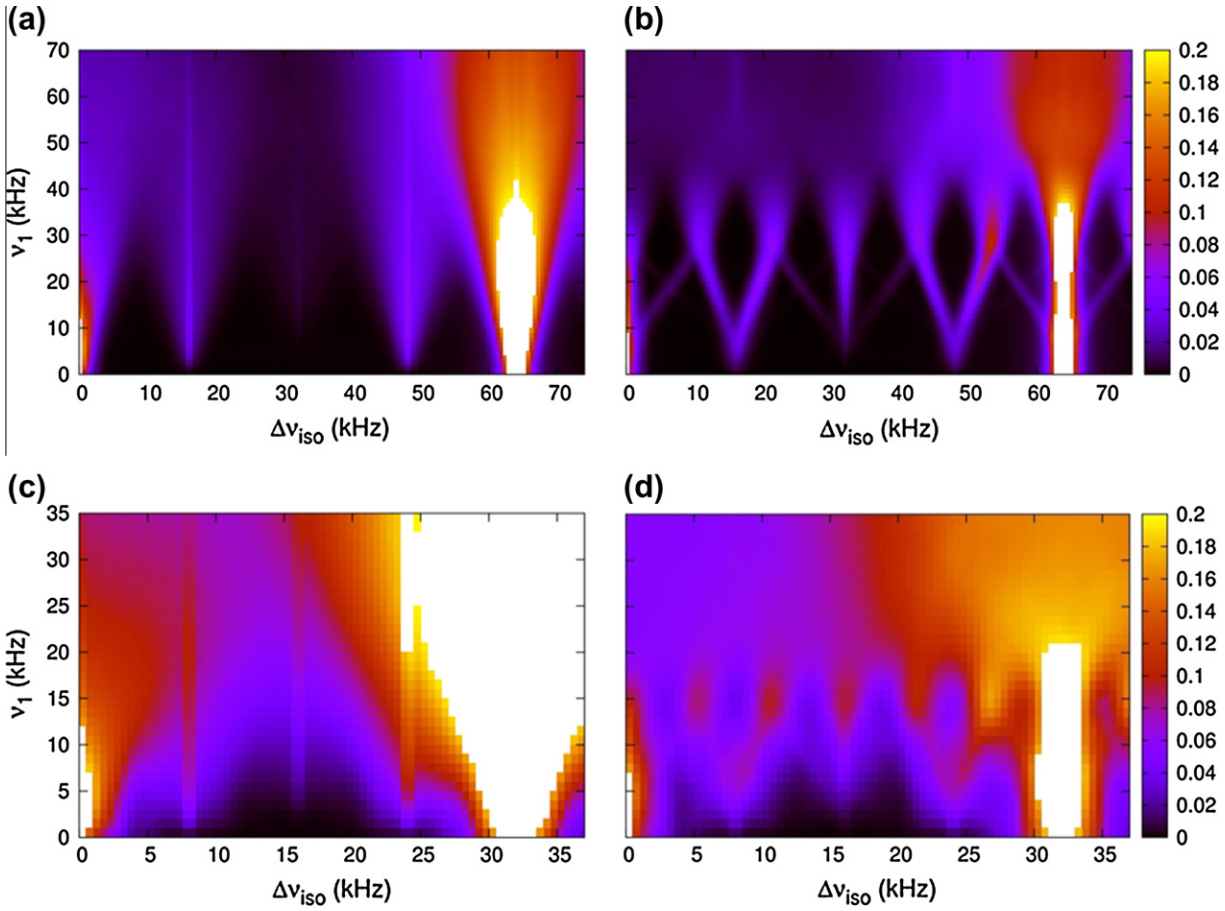

Fig. 5. Recoupling efficiency of the sequences versus the rf-field amplitude, ν_1, and the carbon frequency difference, $\Delta\nu_{iso}$, with $\nu_R = 64$ (a and b) or 32 (c and d) kHz. The ^{13}C–^{13}C recoupling sequences are (a and c) PARIS$_{xy}$ ($m = 2$) and (b and d) SHANGHAI. The spin- system is C1H–C2H$_2$–H$_2$. This figure should be compared with Fig. 4.

efficiencies of PARIS$_{xy}$ ($m = 2$) and SHANGHAI methods at $\nu_1 = 36$ kHz is shown in Fig. S1d. This figure demonstrates that PARIS$_{xy}$ ($m = 2$) benefits from higher efficiency at the ZB and broader R^{2}B condition than SHANGHAI. In contrast, SHANGHAI method is complementary of PARIS$_{xy}$ ($m = 2$) since it displays five SBs at $\Delta\nu_{iso}$ values where PARIS$_{xy}$ ($m = 2$) is inefficient.

Globally, at $\nu_R = 64$ kHz, the ^{13}C recoupling sequences present in the interval of $\Delta\nu_{iso} = 0$–40 kHz useful for high magnetic fields, the following number of SBs: zero for PDSD and PARIS (see Fig. 3a and c), one for PARIS$_{xy}$ ($m = 1$ and 2) (see Figs. 3d and 4a), two for DARR/RAD (see Fig. 3b) and four for SHANGHAI (see Fig. 4b). However, even in the case of the SHANGHAI sequence, which displays the largest number of SBs, there is always $\Delta\nu_{iso}$ values in the interval [0, 40 kHz] for which the magnetization transfer is inefficient. A solution consists in the use of a lower MAS speed, only slightly larger than the maximum value, $\Delta\nu_{iso}^{max}$. This condition allows matching the correlation of peaks with maximum frequency difference with the R^{2}B condition and shifting all the SBs in the relevant interval [0, $\Delta\nu_{iso}^{max}$]. The exact matching, $\Delta\nu_{iso}^{max} = \nu_R$, should be avoided in order to prevent the line-broadening occurring at exact R^{2}B condition. Therefore, the best MAS frequency at $B_0 = 21.1$ T should be about $\nu_R = 40$ kHz.

Furthermore, while the R^{2}B condition reintroduces the dipolar interaction in the first-order effective Hamiltonian, the ZB and SBs only reintroduce the dipolar interaction in the second-order terms [35]. The magnitude of second-order terms is inversely proportional to the MAS speed and hence, to obtain the same transfer efficiency, the mixing time is proportional to the ν_R value. Fig. S1d and e shows the difference of recoupling mechanisms between R^{2}B and ZB/SB conditions. For a given mixing time, $\tau_{mix} = 250$ ms, the efficiency of R^{2}B condition is unaffected by a doubling of the MAS speed, whereas the efficiency of ZB/SB conditions exhibits a twofold decrease between $\nu_R = 32$ and 64 kHz. Consequently, SHANGHAI, PARIS and PARIS$_{xy}$ methods should result in more efficient recoupling at $\nu_R = 40$ than at 64 kHz.

In the following, we focus on PARIS$_{xy}$ ($m = 2$) and SHANGHAI since these methods present the largest numbers of SBs and hence the lowest dependence on the rf-amplitude ν_1.

2.2. C1H–C2 spin-system under fast MAS

In this section, we investigate the efficiency of PARIS$_{xy}$ ($m = 2$) and SHANGHAI at MAS speed of 32 kHz. With respect to ultra-fast MAS, $\nu_R = 32$ kHz is advantageous since it is compatible with the use of bigger rotors and the efficiency of ZB and SBs is inversely proportional to the speed. Both these features contribute to enhance the sensitivity. A drawback can be a loss in spectral resolution for C′–C^{al} correlation matching the exact R^{2}B condition (Fig. 1). In Fig. 4c and d we have simulated the efficiency versus $\Delta\nu_{iso}$, which can be obtained at $\nu_R = 32$ kHz, with PARIS$_{xy}$ ($m = 2$) and SHANGHAI. Two rows of Fig. 4c and d are extracted and shown in Fig. S1e. As already stated, the comparison of Fig. S1d and e shows that lower MAS speed results in higher efficiency for the ZB and SBs since they correspond to second-order recoupling. As the ZB, SB and R^{2}B conditions cover a narrower $\Delta\nu_{iso}$ interval at $\nu_R = 32$ kHz and their widths are slightly modified by MAS frequency (Fig. S1), the average recoupling efficiency of PARIS$_{xy}$ ($m = 2$) and SHANGHAI over the interval [0, $\Delta\nu_{iso}^{max}$] is higher at

ν_R = 32 kHz than at ν_R = 64 kHz. As already observed at ν_R = 64 kHz, the widths of all the recoupling conditions increase with rf-amplitude ν_1. However, mixing times are always in the order of several hundred milliseconds, especially when observing long distance cross-peaks, and it may thus be dangerous practically to use too large rf-amplitudes, which may destroy the proteins.

PARIS$_{xy}$ (m = 2) and SHANGHAI are complementary since their SBs cover different $\Delta\nu_{iso}$ intervals. SHANGHAI displays a larger number of SBs, but both methods are inefficient for some $\Delta\nu_{iso}$ values. Furthermore, lower rf-amplitudes are required at ν_R = 32 kHz since Fig. 4 shows that the width of the recoupling conditions depends on the ratio ν_1/ν_R and in the case of SHANGHAI, the best distributed SB positions are obtained when $\nu_1 \approx \nu_R/2$, also called HORROR condition.

2.3. C1H–C2H$_2$–H$_2$ spin-system under fast and ultra-fast MAS

Previous simulations have been performed with a single-proton C1H–C2 spin-system, disregarding CSA and ^{1}H–^{1}H dipolar interaction. This over-simplified spin-system is rarely encountered in biomolecules. The effect of ^{1}H–^{1}H dipolar homo-nuclear interactions was investigated by performing numerical simulations of recoupling efficiency for PARIS$_{xy}$ (m = 2) and SHANGHAI methods in the case of C1H–C2H$_2$–H$_2$ spin system. The results corresponding to ν_R = 32 and 64 kHz are shown in Fig. 5.

The efficiencies calculated with (Fig. 5a and b) and without (Fig. 4a and b) ^{1}H–^{1}H interactions at ν_R = 64 kHz are similar and they only differ by a small broadening of the recoupling bands. The smallness of the differences is related to the large attenuation of the ^{1}H–^{1}H dipolar interactions at ultra-fast MAS. This is not the case at ν_R = 32 kHz, where the widths of recoupling conditions strongly differ from those calculated previously (compare Figs. 5c, d, 4c, and d). This broadening of recoupling conditions arising from ^{1}H–^{1}H dipolar interactions has already been described in the case of DARR and PARIS$_{xy}$ [24,27]. In addition, at ν_R = 32 kHz, a third recoupling SB at $\Delta\nu_{iso} = \nu_R/2$ appears for PARIS$_{xy}$ (m = 2). With this more realistic spin-system, one thus observes a relatively continuous recoupling (zones that are not in black) for $\Delta\nu_{iso}$ going from zero to ν_R, as long as the rf-field is larger than c.a. 10 kHz for SHANGHAI and 15 kHz for PARIS$_{xy}$. Nevertheless, even in the presence of ^{1}H–^{1}H dipolar interactions, the recoupling conditions of PARIS$_{xy}$ (m = 2) and SHANGHAI are still complementary.

3. Experimental verifications

Experimental verifications were performed on Bruker AVANCE-III 800, 900 and 1000 spectrometers with B_0 = 18.8, 21.1 and 23.5 T, respectively. Commercial Bruker double-resonance ∅ = 1.3 mm MAS probes, which permit spinning frequencies of up to ν_R = 70 kHz, were used for all experiments. Using the same probe, the same sample volume and the same mixing time of τ_{mix} = 250 ms at fast and ultra-fast MAS, allows an easy quantitative comparison of the transfer efficiencies. Typical 90° pulse lengths were 2 μs on both channels. The contact time for cross-polarization was 3 ms, and PISSARRO [36] proton dipolar decoupling was used during evolution and detection periods. Recycle delays were 3 s for all experiments. Additional experimental details are given in the figure captions.

Experiments were performed on samples of L-[U–^{13}C]-histidine·HCl·H$_2$O with 99% ^{13}C purity, which were purchased from CortecNet and used without purification.

SHANGHAI and PARIS$_{xy}$ (m = 2) were first compared experimentally at 18.8 T with two different spinning speeds: ν_R = 32 kHz with ν_1 = 18 kHz and ν_R = 64 kHz with ν_1 = 36 kHz. The corresponding 2D spectra are displayed in Figs. S2, S3a, and b, respectively. It must be reminded that only the cross-peaks, not the auto-peaks, are meaningful in this type of experiments. By comparing the cross-peak intensities, one observes a much larger sensitivity at ν_R = 32 kHz with respect to ν_R = 64 kHz; which is consistent with the simulations shown in Figs. 4 and 5, and S1. The rows along F_2 axis corresponding to the six carbon peaks in the spectra of Fig. S2 (ν_R = 32 kHz) are shown in Fig. 6. In this figure, the intensities of most cross-peaks are higher in the case of SHANGHAI, and we observe at least a twofold enhancement for twelve cross-peaks out of the 30 ones. PARIS$_{xy}$ (m = 2) produces higher intensity for the two pairs of cross-peaks C^4–C^5 and C′–C$^\beta$, which correspond to $\Delta\nu_{iso}$ = 1.7 kHz and 29 kHz, respectively. These experimental results agree with the numerical simulations, which show that PARIS$_{xy}$ (m = 2) shows a higher efficiency around the ZB and R^{2}B conditions.

Fig. S3 also shows that the HORROR condition ($\nu_1 \approx \nu_R/2$) is the most efficient to promote the magnetization transfer among the carbon nuclei, especially for the SHANGHAI method. This is verified experimentally at ν_R = 64 kHz by comparing the cross-peaks observed with ν_1 = 64 (Fig. S3c and d) or 18 (Fig. S3e and f) kHz, with those recorded with ν_1 = 36 kHz (Fig. S3a and b). This experimental result again agrees with the numerical simulations shown in Fig. 5a and b. Indeed, the HORROR condition has the advantage of combining significant efficiency and broadening of the recoupling conditions. For $\nu_1 > \nu_R/2$, the efficiency of the recoupling conditions decreases, whereas for $\nu_1 < \nu_R/2$, the width of the recoupling condition decreases. The broadening of the recoupling around the HORROR condition arises from the reintroduction of ^{1}H–^{1}H dipolar interactions, which are averaged out by ultra-fast MAS. Fig. S3c and d shows that the R^3 condition ($\nu_1 \approx \nu_R$) is less efficient than the HORROR condition to promote magnetization transfer in the case of PARIS$_{xy}$ (m = 2) and SHANGHAI at ultra-fast MAS.

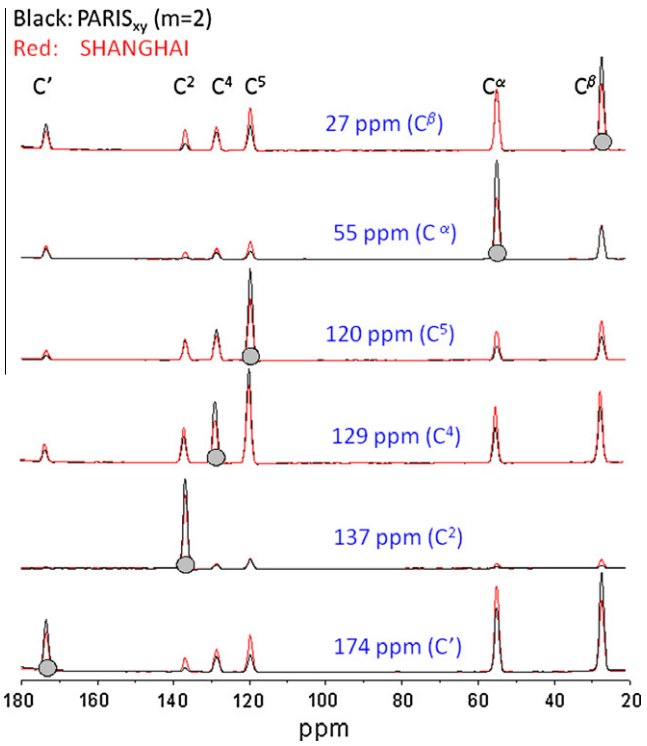

Fig. 6. 1D rows extracted from 2D spectra shown in Fig. S2a and b and recorded at 18.8 T with ν_R = 32 kHz, ν_1 = 18 kHz and τ_{mix} = 250 ms. Un-informative auto-peaks are indicated by filled circles at their feet. PARIS$_{xy}$ is shown with black curve and SHANGHAI with red curve. (For interpretation of the references to color in this figure legend, the reader is referred to the web version of this article.)

In a general way, at fast MAS ($\nu_R \approx 30$–35 kHz), we have always observed experimentally that an rf-field close to the HORROR condition ($\nu_1 \approx \nu_R/2$) always gives the best compromise in terms of efficiency and dissipated rf-power.

In Fig. 7, we show the 2D spectra of both sequences recorded at 23.5 T. The spinning speed, $\nu_R = 40$ kHz, has been chosen slightly larger than the maximum carbon frequency range $\Delta\nu_{iso}^{max} = 38$ kHz. This choice allows matching $\Delta\nu_{iso}^{max}$ with the R^2B condition and using a rotor-synchronized experiment ($t_1 = kT_R$), which avoids spinning sidebands along F_1, hence simplifying the spectrum. All cross-peaks are larger with SHANGHAI than with PARIS$_{xy}$ ($m = 2$), even those close to the diagonal, which

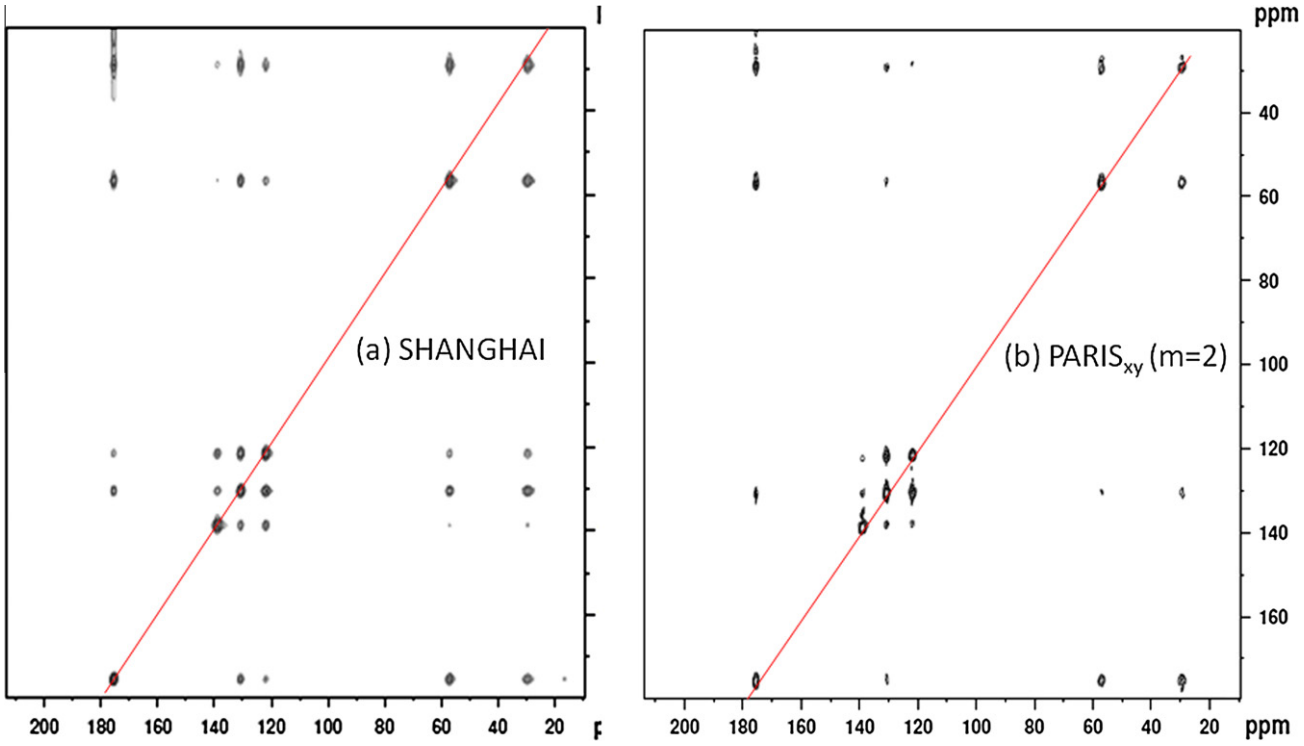

Fig. 7. Experimental ^{13}C–^{13}C correlation maps of histidine recorded at 23.5 T with $\nu_R = 40$ kHz, $\nu_1 = 15$ kHz and $\tau_{mix} = 250$ ms. The ^{13}C–^{13}C recoupling sequences are (a) SHANGHAI and (b) PARIS$_{xy}$ ($m = 2$). Only 28 complex t_1 points have been recorded with States-TPPI, which leads to F_1 truncation. The experiment time to record each spectrum was 23 min.

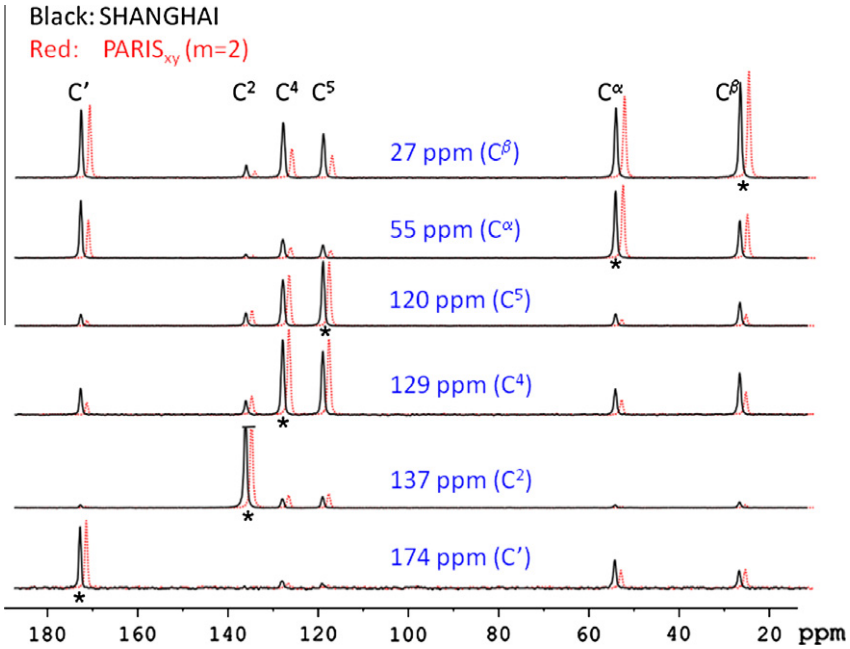

Fig. 8. 1D rows extracted from 2D spectra recorded at 21.1 T with $\nu_R = 40.5$ kHz $= 1/\Delta t_1$, $\nu_1 = 20$ kHz and $\tau_{mix} = 250$ ms. Un-informative auto-peaks are indicated by * at their feet. PARIS$_{xy}$ ($m = 2$) is shown with red dashed curves and SHANGHAI with black curves. 280 complex t_1 points have been recorded with States-TPPI, which leads to an experiment time of 230 min for each spectrum. (For interpretation of the references to color in this figure legend, the reader is referred to the web version of this article.)

corresponds to the ZB condition. SHANGHAI is especially more efficient for cross-peaks with $\Delta\nu_{iso}$ values in the interval $[\nu_R/3, 2\nu_R/3]$ = [13, 26 kHz], which corresponds mainly to cross-peaks involving one aromatic carbon nucleus (Fig. 1). It is important to note that even with only 1.5 μl of sample (∅ = 1.3 mm), and with a very short acquisition time of 23 min, we have been able to see all cross-peaks. We even observe those related to inter-molecular magnetization exchange, such as C^2–C' with $r(C^2–C') \approx 4.05$ Å and $\Delta\nu_{iso}$ = 9.25 kHz, or C^2–C^α with $r(C^2–C^\alpha) \approx 4.6$ Å and $\Delta\nu_{iso}$ = 20.5 kHz. This contribution should disappear with a sample diluted by natural abundance histidine.

We have also recorded the 2D spectra of both sequences at 21.1 T, but with rf and spinning speed specifications optimized for PARIS$_{xy}$ (m = 2) [27]. Indeed, in this case, the speed has been chosen to promote simultaneously under PARIS$_{xy}$ (m = 2) the magnetization transfer between aliphatic (≈40 ppm) and aromatic (≈130 ppm) carbons ($\Delta\nu_{iso}$ = 90 ppm ≈ 20.3 kHz) and between aliphatic and carboxyl carbons ($\Delta\nu_{iso}$ = 174–40 = 135 ppm ≈ 30.5 kHz). The only way to match simultaneously both transfers with PARIS$_{xy}$ (m = 2) is to use the two recoupling bands at $\nu_R/2$ and $3\nu_R/4$ (Fig. 5c). In order for these two modulation bands to recouple optimally and simultaneously all cross-peaks, the spinning speed has thus been fixed to ν_R = 40.5 kHz ≈ 2 ∗ 20.3 kHz ≈ 1.333 ∗ 30.5 kHz. The third recoupling modulation at $\Delta\nu_{iso} = \nu_R/4$ can help the exchange between spectrally closer carboxyl and aromatic regions. The rf-field has been fixed to its previously used condition for PARIS$_{xy}$ (m = 2) to ν_1 = 20 kHz [27]. The rows of the 2D spectra are presented in Fig. 8. At least 16 cross-peaks display larger intensities for SHANGHAI than for PARIS$_{xy}$ (m = 2). However, ten cross-peaks display larger intensities in the case of PARIS$_{xy}$ (m = 2); those with $\Delta\nu_{iso} \leqslant 6.2$ kHz (C^2–C^4, C^4–C^5, C^2–C^5, C^α–C^β) and $\Delta\nu_{iso} \geqslant 33$ kHz (C'–C^β). This observation agrees with numerical simulations, which show that PARIS$_{xy}$ (m = 2) is more efficient than SHANGHAI around ZB and R^2B conditions, whereas otherwise SHANGHAI is more efficient than PARIS$_{xy}$ (m = 2).

However, it must be noted that at very high magnetic fields, the optimum conditions for PARIS$_{xy}$ (m = 2) lead to spinning speeds that are only available with very small rotor diameters (∅ ⩽ 1.3 mm), thus leading to very small sample volumes. As example, with histidine ($\Delta\nu_{iso}^{max}$ = 135 ppm), the spinning speed is then related to the proton Larmor frequency by ν_R (Hz) ≈ 45ν_{0H} (MHz). This means that a small rotor diameter (∅ ⩽ 1.3 mm) must be used as long as the magnetic field is larger than 17 T. On the contrary, due to the larger number of SBs, optimum conditions for SHANGHAI are more 'broad-banded' from the speed point of view, and spectra can be recorded optimally with a 2.5 mm ∅ rotor, even at very high magnetic fields, which leads to much larger S/N ratio, due to larger sample volume and increased efficiency.

4. Conclusion

There are two types of methods for structural analyzes of biomolecules, which are based either on first- or on second-order transfer schemes. Actually, the two types of methods are complementary. Indeed, first-order methods mainly give access to one-bond correlations, thus allowing the protein skeleton to be assigned easily [10b] while second-order ^{1}H assisted methods permit observing longer distance contacts, thus allowing the observation of protein folding.

We have proposed a broadband super-cycled four-phase dipolar recoupling scheme, SHANGHAI, for second-order ^{1}H assisted ^{13}C–^{13}C correlation experiments. This method, which has been demonstrated at the very high magnetic field of 23.5 T, complements the previous recoupling schemes, especially the PARIS$_{xy}$ (m = 2) sequence [27]. The efficiencies of the two methods have been compared in the present article. PARIS$_{xy}$ is more efficient around ZB ($\Delta\nu_{iso} \approx 0$) and R^2B ($\Delta\nu_{iso} \approx \nu_R$) conditions, whereas SHANGHAI exhibits higher efficiency for intermediate conditions owing to a larger number of SBs. For both SHANGHAI and PARIS$_{xy}$ (m = 2), the optimal speed ν_R is slightly superior to the largest $\Delta\nu_{iso}^{max}$ value in order to benefit from the R^2B recoupling, while avoiding the line broadening produced at the exact R^2 condition $\Delta\nu_{iso} = \nu_R$. At $B_0 \geqslant 17$ T, $\Delta\nu_{iso}^{max}$ is larger than 35 kHz, and hence also the optimal MAS speed. Therefore, rotors with outer diameters strictly smaller than 2.5 mm must then be used. However, owing to a larger number of SBs, SHANGHAI benefits from a better flexibility in the choice of MAS frequency than PARIS$_{xy}$ (m = 2) and was demonstrated to be more efficient at ν_R = 32 and 64 kHz. Experiments at ν_R = 30–35 kHz allow an enhancement in sensitivity since they are compatible with larger rotor outer diameter (2.5 mm for instance) and they benefit from a faster magnetization transfer for these second-order dipolar recoupling methods. Nevertheless, when $\nu_R < \Delta\nu_{iso}^{max}$, the MAS frequency must be carefully chosen to avoid the exact R^2 condition for any ^{13}C resonance pairs. This is easy for small organic molecules exhibiting a limited number of resonances, but is more difficult in the case of proteins.

Whatever the spinning speed, the HORROR condition ($\nu_1 \approx \nu_R/2$) produces the most uniform recoupling distribution in SHANGHAI experiment. At ultra-fast MAS (ν_R > 60 kHz), the SHANGHAI method is only efficient close to this HORROR condition. Conversely, at moderate to fast MAS (ν_R = 20–35 kHz), it can be used with any rf-amplitude larger than ν_1 > 10 kHz (see Fig. 5d), which prevents potentially damaging heating of the sample.

As the recoupling conditions of SHANGHAI and PARIS$_{xy}$ (m = 2) complement each other (see Fig. 5c and d), it may be possible to combine sequentially the two super-cyclings to excite more uniformly the carbon frequency range.

These two methods, which only use ^{1}H irradiation during mixing time, can be complemented with another second-order method, PAR, which irradiates simultaneously the ^{1}H and ^{13}C channels and is very efficient at ultra-fast MAS [37].

Owing to their limited sensitivity to dipolar truncation, all second-order methods are especially useful to the analysis of long-range distances, which can be used to determine the folding of the protein. Nevertheless, the dipolar truncation is not fully cancelled out with these sequences. Therefore, determination of accurate distances is problematic, because (i) the geometry of the two carbons and their local surroundings, including the protons and other carbons, should be taken into account for distance determination and (ii) cross-peaks related to long distances are often mixtures of direct and relayed polarization transfers [38,39], which strongly complicates the simulations. Nevertheless, it has very recently been shown that 'transfer efficiency of PARIS$_{xy}$ (m = 2) reveals a linear dependence on the strength of the dipolar coupling, which permits one to relate weak cross-peak intensities with long distances' [27a]. A similar behavior is anticipated for SHANGHAI.

It must be reminded that another way to increase the efficiency of these homo-nuclear methods is to reduce their experimental time by decreasing the number of t_1 steps required to acquire the spectra without loss of resolution along F_1. This can be obtained by using a covariance data treatment, either with uniform [40] or non-uniform [10a,41] indirect sampling.

Moreover, SHANGHAI and PARIS$_{xy}$ (m = 2) can be used to access in a quantitative way to thermal equilibrium magnetizations in single-pulse [42] or CP [43] MAS experiments.

Acknowledgments

Authors have greatly appreciated the comments of the two reviewers, which greatly improved the quality of the manuscript.

They are also grateful for funding provided by Region Nord/Pas de Calais, Europe (FEDER), CNRS, French Minister of Science, USTL, ENSCL, CortecNet and Bruker BIOSPIN. Financial support from the TGIR RMN THC (FR-3050) for conducting the research is gratefully acknowledged. B. Hu is thankful for the funding supported by "the Fundamental Research Funds for the Central Universities". Q. Chen is grateful for the National fundamental research program 2007CB925200, Shanghai Leading Talent Training Program. Authors also thank Contract ANR-2010-jcjc-0811-01.

Appendix A. Supplementary material

Supplementary data associated with this article can be found, in the online version, at doi:10.1016/j.jmr.2011.07.011.

References

[1] F. Castellani, B. van Rossum, A. Diehl, M. Schubert, K. Rehbein, H. Oschkinat, Structure of a protein determined by solid-state magic-angle-spinning NMR spectroscopy, Nature 420 (2002) 98–102.
[2] A. Lange, S. Becker, K. Seidel, K. Giller, O. Pongs, M. Baldus, A concept for rapid protein-structure determination by solid-state NMR spectroscopy, Angew. Chem., Int. Ed. 44 (2005) 2089–2092;
A. Lange, K. Giller, S. Hornig, M.F. Martin-Eauclaire, O. Pongs, S. Becker, M. Baldus, Toxin-induced conformational changes in a potassium channel revealed by solid-state NMR, Nature 440 (2006) 959–962.
[3] A. Goldbourt, B.J. Cross, A.L. Day, A.E. McDermott, Filamentous phage studied by magic-angle spinning NMR: resonance assignment and secondary structure of the coat protein in Pf1, J. Am. Chem. Soc. 129 (2007) 2338–2344.
[4] C. Wasmer, A. Lange, H. Van Melckebeke, A.B. Siemer, R. Riek, B.H. Meier, Amyloid fibrils of the HET-s (218–289) Prion form a β solenoid with a triangular hydrophobic core, Science 319 (2008) 1523–1526.
[5] (a) M. Hohwy, C.M. Rienstra, C.P. Jaroniec, R.G. Griffin, Fivefold symmetric homo-nuclear dipolar recoupling in rotating solids: application to double quantum spectroscopy, J. Chem. Phys. 110 (1999) 7983–7992;
(b) R. Schneider, K. Seidel, M. Etzkorn, A. Lange, S. Becker, M. Baldus, Probing molecular motion by double-quantum (^{13}C,^{13}C) solid-state NMR spectroscopy: application to ubiquitin, J. Am. Chem. Soc. 132 (2010) 223–233.
[6] K.Y. Huang, A.B. Siemer, A.E. McDermott, Homo-nuclear mixing sequences for perdeuterated proteins, J. Magn. Reson. 208 (2011) 122–127.
[7] M. Ernst, M.A. Meier, T. Tuherm, A. Samoson, B.H. Meier, Low-power high-resolution solid-state NMR of peptides and proteins, J. Am. Chem. Soc. 126 (2004) 4764–4765.
[8] G. De Paepe, J.R. Lewandowski, R.G. Griffin, Spin dynamics in the modulation frame: application to homo-nuclear recoupling in magic angle spinning solid-state NMR, J. Chem. Phys. 129 (2008) 245101.
[9] (a) Y. Ishii, ^{13}C–^{13}C dipolar recoupling under very fast magic angle spinning in solid-state nuclear magnetic resonance: applications to distance measurements, spectral assignments, and high-throughput secondary-structure determination, J. Chem. Phys. 114 (2001) 8473–8483;
(b) K. Riedel, C. Herbst, J. Leppert, O. Ohlenschläger, M. Görlach, R. Ramachandran, Broadband homo-nuclear double-quantum NMR filtering via zero-quantum dipolar recoupling in rotating solids, Chem. Phys. Lett. 424 (2006) 178–183;
(c) M.J. Bayro, R. Ramachandran, M.A. Caporini, M.T. Eddy, R.G. Griffin, Radio frequency-driven recoupling at high magic-angle spinning frequencies: homo-nuclear recoupling sans hetero-nuclear decoupling, J. Chem. Phys. 128 (2008) 052321.
[10] (a) B. Hu, L. Delevoye, O. Lafon, J. Trébosc, J.P. Amoureux, Double-quantum NMR spectroscopy of ^{31}P species submitted to very large CSAs, J. Magn. Reson. 200 (2009) 178–188;
(b) O. Lafon, J. Trébosc, B. Hu, G. De Paëpe, J.P. Amoureux, Observing ^{13}C–^{13}C connectivities at high magnetic field and very high spinning frequencies, Chem. Commun. 47 (2011) 6930–6932.
[11] (a) M. Baldus, B.H. Meier, Broadband polarization transfer under magic-angle spinning: application to total through-space-correlation NMR spectroscopy, J. Magn. Reson. 128 (1997) 172–193;
(b) M.J. Bayro, M. Huber, R. Ramachandran, T.C. Davenport, B.H. Meier, M. Ernst, R.G. Griffin, Dipolar truncation in magic-angle spinning NMR recoupling experiments, J. Chem. Phys. 130 (2009) 114506.
[12] V. Ladizhansky, Homo-nuclear dipolar recoupling techniques for structure determination in uniformly ^{13}C-labeled proteins, Solid State Nucl. Magn. Reson. 36 (2009) 119–128.
[13] D.P. Raleigh, M.H. Levitt, R.G. Griffin, Rotational resonance in solid state NMR, Chem. Phys. Lett. 146 (1988) 71–76;
M.G. Colombo, B.H. Meier, R.R. Ernst, Rotor-driven spin diffusion in natural-abundance ^{13}C spin systems, Chem. Phys. Lett. 146 (1988) 189–196;
K. Takegoshi, K. Nomura, T. Terao, Rotational resonance in the tilted rotating frame, Chem. Phys. Lett. 232 (1995) 424–428;
R. Ramachandra, V. Ladizhansky, V.S. Bajaj, R.G. Griffin, ^{13}C–^{13}C rotational resonance width distance measurements in uniformly ^{13}C-labeled peptides, J. Am. Chem. Soc. 125 (2003) 15623.
[14] G. De Paepe, J.R. Lewandowski, R.G. Griffin, Spin dynamics in the modulation frame: application to homo-nuclear recoupling in magic angle spinning solid-state NMR, J. Chem. Phys. 128 (2008) 124503.
[15] A.K. Paravastu, R. Tycko, Frequency-selective homo-nuclear dipolar recoupling in solid state NMR, J. Chem. Phys. 124 (2006) 194303.
[16] I. Scholz, M. Huber, T. Manolikas, B.H. Meier, M. Ernst, MIRROR recoupling and its application to spin diffusion under fast magic-angle spinning, Chem. Phys. Lett. 460 (2008) 278–283.
[17] I. Marin-Montesinos, G. Mollica, M. Carravetta, A. Gansmuller, G. Pilelo, M. Bechmann, A. Sebald, M.H. Levitt, Truncated dipolar recoupling in solid-state nuclear magnetic resonance, Chem. Phys. Lett. 432 (2006) 572–578.
[18] N. Khaneja, N.C. Nielsen, Triple oscillating field technique for accurate distance measurements by solid-state NMR, J. Chem. Phys. 128 (2008) 015103;
L.A. Straasø, M. Bjerring, N. Khaneja, N.C. Nielsen, Multiple-oscillating-field techniques for accurate distance measurements by solid-state NMR, J. Chem. Phys. 130 (2009) 225103.
[19] K.N. Hu, R. Tycko, Zero-quantum frequency-selective recoupling of homo-nuclear dipole–dipole interactions in solid-state nuclear magnetic resonance, J. Chem. Phys. 131 (2009) 045101.
[20] R. Tycko, Theory of stochastic dipolar recoupling in solid-state nuclear magnetic resonance, J. Phys. Chem. B 112 (2008) 6114–6121;
R. Tycko, Stochastic dipolar recoupling in nuclear magnetic resonance of solids, Phys. Rev. Lett. 99 (2007) 187601.
[21] N.M. Szeverenyi, M.J. Sullivan, G.E. Maciel, Observation of spin exchange by two-dimensional Fourier transform ^{13}C cross-polarization magic-angle spinning, J. Magn. Reson. 47 (1982) 462–475.
[22] A. Grommek, B.H. Meier, M. Ernst, Distance information from proton-driven spin diffusion under MAS, Chem. Phys. Lett. 427 (2006) 404–409.
[23] B.H. Meier, Polarization transfer and spin diffusion in solid state NMR, in: W.S. Warren (Ed.), Advances in Magnetic and Optical Resonance, vol. 18, Academic Press, New York, 1994, p. 1.
[24] (a) K. Takegoshi, S. Nakamura, T. Terao, ^{13}C–^{1}H dipolar-assisted rotational resonance in magic-angle spinning NMR, Chem. Phys. Lett. 344 (2001) 631–637;
(b) K. Takegoshi, S. Nakamura, T. Terao, ^{13}C–^{1}H dipolar-driven ^{13}C–^{13}C recoupling without ^{13}C rf irradiation in nuclear magnetic resonance of rotating solids, J. Chem. Phys. 118 (2003) 2325–2341.
[25] C.R. Morcombe, V. Gaponenko, R.A. Byrd, K.W. Zilm, Diluting abundant spins by isotope edited radio-frequency field assisted diffusion, J. Am. Chem. Soc. 126 (2004) 7196–7197.
[26] (a) L. Duma, D. Abergel, F. Ferrage, P. Pelupessy, P. Tekely, G. Bodenhausen, Broadband dipolar recoupling for magnetization transfer in solid-state NMR correlation spectroscopy, Chem. Phys. Chem. 9 (2008) 1104–1106;
(b) M. Weingarth, D.E. Demco, G. Bodenhausen, P. Tekely, Improved magnetization transfer in solid-state NMR with fast magic angle spinning, Chem. Phys. Lett. 469 (2009) 342–348;
(c) M. Weingarth, G. Bodenhausen, P. Tekely, Broadband carbon-13 correlation spectra of micro crystalline proteins in very high-magnetic fields, J. Am. Chem. Soc. 131 (2009) 13937–13939.
[27] (a) M. Weingarth, G. Bodenhausen, P. Tekely, Broadband magnetization transfer using moderate radio-frequency fields for NMR with very high static fields and spinning speeds, Chem. Phys. Lett. 488 (2010) 10–16;
(b) M. Weingarth, Y. Masuda, K. Takegoshi, G. Bodenhausen, P. Tekely, Sensitive ^{13}C–^{13}C correlation spectra of amyloid fibrils at very high spinning frequencies and magnetic fields, J. Biomol. NMR 50 (2011) 129–136.
[28] G. Hou, S. Yan, S. Sun, Y. Han, I.J.L. Byeon, J. Ahn, J. Concel, A. Samoson, A.M. Gronenborn, T. Polenova, Spin diffusion driven by R-symmetry sequences: applications to homo-nuclear correlation spectroscopy in MAS NMR of biological and organic solids, J. Am. Chem. Soc. 133 (2011) 3943–3953.
[29] M. Veshtort, R.G. Griffin, SPINEVOLUTION: a powerful tool for the simulation of solid and liquid state NMR experiments, J. Magn. Reson. 178 (2006) 248–282.
[30] M. Bak, N.C. Nielsen, REPULSION: a novel approach to efficient powder averaging in solid-state NMR, J. Magn. Reson. 125 (1997) 132–139.
[31] (a) M. Ernst, A. Samoson, B.H. Meier, Low-power decoupling in fast magic-angle spinning NMR, Chem. Phys. Lett. 348 (2001) 293–302;
(b) M. Ernst, A. Samoson, B.H. Meier, Low-power XiX decoupling in MAS NMR experiments, J. Magn. Reson. 163 (2003) 332–339;
(c) S. Laage, J.R. Sachleben, S. Steuernagel, R. Pieratelli, G. Pintacuda, L. Emsley, Fast acquisition of multi-dimensional spectra in solid-state NMR enabled by ultra-fast MAS, J. Magn. Reson. 196 (2009) 133–141.
[32] Y. Ishii, R. Tycko, Sensitivity enhancement in solid-state ^{15}N NMR by indirect detection with high-speed magic angle spinning, J. Magn. Reson. 142 (2000) 199–204.
[33] (a) Y. Ishii, N.P. Wickramasinghe, S. Chimon, A new approach in 1D and 2D ^{13}C high-resolution solid-state NMR spectroscopy of paramagnetic organometallic complexes by very fast magic-angle spinning, J. Am. Chem. Soc. 125 (2003) 3438–3439;
(b) I. Bertini, L. Emsley, M. Lelli, C. Luchinat, J. Mao, G. Pintacuda, Ultra-fast MAS solid-state NMR permits extensive ^{13}C and ^{1}H detection in paramagnetic metalloproteins, J. Am. Chem. Soc. 132 (2010) 5558–5559.
[34] (a) T.G. Oas, R.G. Griffin, M.H. Levitt, Rotary resonance recoupling of dipolar interactions in solid-state nuclear magnetic resonance spectroscopy, J. Chem. Phys. 89 (1988) 692–695;

(b) M.H. Levitt, T.G. Oas, R.G. Griffin, Rotary resonance recoupling in hetero-nuclear spin pair systems, Israel J. Chem. 28 (1988) 271–282;
(c) N.C. Nielsen, H. Bildsoe, H.J. Jacobsen, M.H. Levitt, Double-quantum homo-nuclear rotary resonance: efficient dipolar recovery in magic-angle spinning nuclear magnetic resonance, J. Chem. Phys. 101 (1994) 1606–1611.

[35] (a) I. Scholz, J.D. van Beek, M. Ernst, Operator-based Floquet theory in solid-state NMR, Solid State Nucl. Magn. Reson. 37 (2010) 39–59;
(b) M. Leskes, Ü. Akbey, H. Oschkinat, B.J. van Rossum, S. Vega, Radio frequency assisted homo-nuclear recoupling, a Floquet description of homo-nuclear recoupling via surrounding hetero-nuclei in fully protonated to fully deuterated systems, J. Magn. Reson. 209 (2011) 207–219.

[36] (a) M. Weingarth, P. Tekely, G. Bodenhausen, Efficient hetero-nuclear decoupling by quenching rotary resonance in solid-state NMR, Chem. Phys. Lett. 466 (2008) 247–251;
(b) M. Weingarth, G. Bodenhausen, P. Tekely, Low-power decoupling at high spinning frequencies in high static fields, J. Magn. Reson. 199 (2009) 238–241;
(c) M. Weingarth, G. Bodenhausen, P. Tekely, Probing the quenching of rotary resonances by PISSARRO decoupling, Chem. Phys. Lett. 502 (2011) 259–265;
(d) M. Weingarth, J. Trébosc, J.P. Amoureux, G. Bodenhausen, P. Tekely, Efficiency at high spinning frequencies of hetero-nuclear decoupling methods designed to quench rotary resonance, Solid State Nucl. Magn. Reson. 40 (2011) 21–26.

[37] G. De Paëpe, J.R. Lewandowski, A. Loquet, A. Bockmann, R.G. Griffin, Proton assisted recoupling and protein structure determination, J. Chem. Phys. 129 (2008) 245101;
J.R. Lewandowski, G. De Paëpe, M.T. Eddy, J. Struppe, W. Maas, R.G. Griffin, Proton assisted recoupling at high spinning frequencies, J. Phys. Chem. B 113 (2009) 9062–9069.

[38] I. Bertini, A. Bhaumik, G. De Paëpe, R.G. Griffin, M. Lelli, J.R. Lewandowski, C. Luchinat, High-resolution solid-state NMR structure of a 17.6 kDa protein, J. Am. Chem. Soc. 132 (2009) 1032–1040.

[39] T. Manolikas, T. Herrmann, B.H. Meier, Protein structure determination from ^{13}C spin-diffusion solid-state NMR spectroscopy, J. Am. Chem. Soc. 130 (2008) 3959–3966.

[40] M. Weingarth, P. Tekely, R. Brüschweiler, G. Bodenhausen, Improving the quality of 2D solid-state NMR spectra of microcrystalline proteins by covariance analysis, Chem. Commun. 46 (2010) 952–954.

[41] O. Lafon, B. Hu, J.P. Amoureux, P. Lesot, Fast and high-resolution stereo-chemical analysis by non-uniform sampling and covariance processing of anisotropic natural abundance 2D ^{2}H NMR datasets, Chem. Eur. J. 17 (2011) 6716–6724.

[42] G. Hou, S. Ding, L. Zhang, F. Deng, Breaking the T_1 constraint for quantitative measurement in magic angle spinning solid-state NMR spectroscopy, J. Am. Chem. Soc. 132 (2010) 5538–5539.

[43] G. Hou, F. Deng, S. Ding, R. Fu, J. Yang, C. Ye, Quantitative cross-polarization NMR spectroscopy in uniformly ^{13}C-labeled solids, Chem. Phys. Lett. 421 (2006) 356–360.